Engineering Covalent Organic Frameworks in the Modulation of Photocatalytic Degradation of Pollutants under Visible Light Conditions

Alicia Jiménez-Almarza,[a] Alberto López-Magano,[a] Rafael Cano,[a] Borja Ortín-Rubio,[b] Diana Díaz-García,[c] Santiago Gomez-Ruiz,[c] Inhar Imaz,[b] Daniel Maspoch,[b,d] Rubén Mas-Ballesté,[a,e,] José Alemán,[e,f,*]*

a. Department of Inorganic Chemistry (Module 7), Facultad de Ciencias, Universidad Autónoma de Madrid, 28049-Madrid, Spain.

b. Catalan Institute of Nanoscience and Nanotechnology (ICN2), CSIC and The Barcelona Institute of Science and Technology, 08193-Barcelona, Spain.

c COMET-NANO Group, Departamento de Biología y Geología, Física y Química Inorgánica, E.S.C.E.T., Universidad Rey Juan Carlos, Calle Tulipán s/n, E-28933 Móstoles, Madrid, Spain.

d. Institució Catalana de Recerca i Estudis Avançats (ICREA), Pg. Lluís Companys 23, 08010-Barcelona, Spain.

e. Institute for Advanced Research in Chemical Sciences (IAdChem), Universidad Autónoma de Madrid, 28049-Madrid, Spain.

f. Department of Organic Chemistry (Module 1), Facultad de Ciencias, Universidad Autónoma de Madrid, 28049-Madrid, Spain.

E-mail: ruben.mas@uam.es, jose.aleman@uam.es. www.uam.es/jose.aleman

Abstract

Mixtures of triphenylamine (TPA) and phenyl phenothiazine (PTH) fragments have been incorporated into a series of extended polyimine structures that have been applied in the photodegradation of pollutants of different nature under visible light irradiation. Results obtained revealed that materials containing PTH as sole photoactive unit resulted the most active photocatalytic material in the degradation of polybrominated diphenyl ether-1 (PBDE-1) and Sudan Red III. In contrast, the COF containing only TPA acted as the best photocatalyst for the degradation of Methylene Blue. These different trends are related to the versatility of PTH moiety to trigger both photoredox and energy transfer processes, while TPA is only an effective energy transfer catalyst.

Keywords: Covalent Organic Frameworks, Photocatalysis, Photodegradation, Pollutants.

1. Introduction

Photocatalysis is a highly promising tool for environmental clean-up and organic synthesis that can result on accelerating photo-activated reactions.[1] Although the photocatalytic scenario is very complex, the two main photocatalytic pathways are energy transfer processes [2] and photoredox reactions.[3] Therefore, to be successful in a photochemical reaction or in the photodegradation of a pollutant, the selection of a photocatalyst able to proceed through an energy transfer or a photoredox pathway is very important. For these reasons, there is a panoply of homogeneous systems based on metal complexes [4] and several organic dyes,[5,6] which are able to perform a wide range of photocatalytic transformations. This variety offers the tool to point towards specific photocatalytic activities under visible-light irradiation.

The difficult recover of homogenous catalysts [7,8] makes heterogeneous systems very desirable because they allow easy separation of the catalyst as well as its recyclability.[9] In addition, the design of materials through combination of suitable building blocks paves the opportunity to tune and direct photocatalytic activity in a manner that is unprecedented for homogeneous catalysis. One strategy that has been employed in the last years is the incorporation of photocatalytic units, normally used in homogeneous catalysis, into porous materials. In particular, reticular materials such as Metal-Organic Frameworks (MOFs) and Covalent Organic Frameworks (COFs) offer many possibilities for their use in photocatalysis.[10,11] As a consequence, photocatalytic applications of reticular materials have been reported in the areas of organic chemical synthesis, degradation of pollutants, CO_2 reduction and water splitting, among others.[12,13]

In recent years, COFs have attracted much attention.[14,15] This emerging family of porous materials are stable laminar or 3D reticular polymeric structures, similar to

MOFs, but only composed by organic linkers connected through covalent bonds. Thus, they are constituted by earth abundant elements, and show low toxicity, low density and adjustable pore size, chemical structure, and functionality. Consequently, applications of COFs have been reported in myriad fields, such as storage and separation of gases,[16] energy storage,[17] drug delivery,[18] proton conduction,[19] optoelectronics [17] and catalysis.[20,21] In the field of catalysis, COFs and their amorphous analogues have also shown to be promising candidates as photocatalysts,[22–29] which performances have been enhanced by incorporating a pre-designed photocatalytic units to the framework, such as benzothiadiazole,[30] benzodifuran,[31] rose Bengal,[32] benzobisthiadiazole,[33] thioxanthone,[34] platinum complex,[35] benzooxadiazole,[36] BODIPY,[37] and azulene.[38]

The versatility of COF materials offers an optimal platform to be applied in the degradation of organic pollutants of different nature.[28] A particular case of persistent organic pollutants (POPs) are polybrominated diphenyl ethers (PBDEs), generally used as flame retardants. Tetra-, penta-, hexa- and heptabromo diphenyl ethers are commonly considered POPs,[39] and evolve generating less brominated derivatives, which are even more toxic and bioaccumulative than the original congeners.[40,41] For this reason, mono-brominated PBDE-1 is widely used as a model substrate to study the photoreduction of polybrominated pollutants that results in hydrodebrominated final products.[42] Synthetic dyes are another class of polluting chemical species commonly used in textile, food or cosmetic industries.[43] Among them, azo dyes are one of the most detrimental class of pollutants because they are highly persistent in the aquatic environment.[44] Sudan dyes, such as Sudan Red III, are common red colored azo dyes used in cosmetics.[45,46] Furthermore, ionic heterocyclic aromatic dyes, such as Methylene Blue, are a harmful class of pollutants, coming from the manufacture of

products related with inkjet printing, photography and xerography, as well as cellulosic and textile industries.[47,48]

The use of different materials attending their preferred catalytic pathways is usually required to achieve the degradation of specific pollutants. Therefore, there is a need of strategies to systematically tune, direct and modulate the photocatalytic activity of predesigned materials. In this work, we targeted this challenge by designing a series of extended polyimine COFs with different combinations of two photoactive units (Figure 1). We selected triphenylamine (TPA) and phenyl phenothiazine (PTH) as photoactive units because they show distinct optical and redox properties. Therefore, they can act as photocatalysts capable of degrading pollutants *via* different pathways.[49,50] In addition, they work as typical trigonal building blocks to construct COFs *via* introduction of aldehyde groups at *para* positions of each phenyl ring. Following this strategy, a series of five 2D COFs **4a-e** with **hcb** (honeycomb) topology and built up from different proportions of TPA and PTH was synthesized by reacting triarylaldehydes **TFPA** (containing TPA as photoactive unit) and/or **3** (containing PTH as photoactive unit) with 1,3,5-tris(4-aminophenyl)benzene (**TAPB**) (Scheme 2). We anticipate that the photocatalytic activity of the resulting COFs, which was essayed for the degradation of three different model pollutants (PBDE-1, Sudan Red III and Methylene Blue) under visible-light conditions, can be modulated by enriching the polyimine structure with one or another photoactive unit (Figure 1).

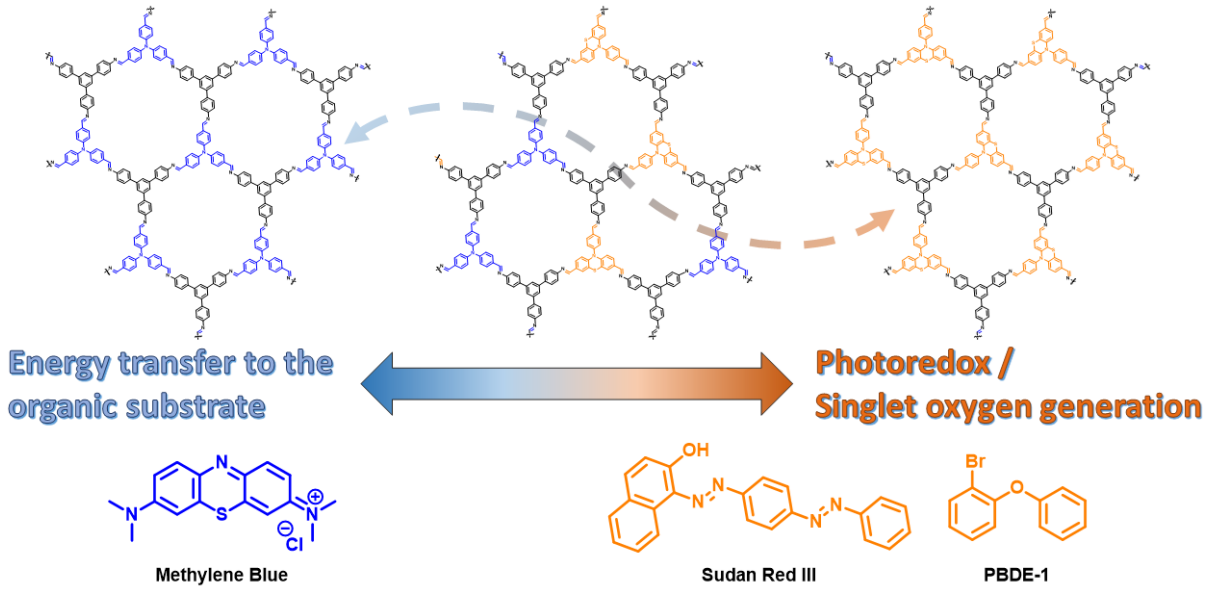

Figure 1. Conceptual idea of this work, modulating the COF isostructural material in photocatalysis.

2. Experimental.

Synthesis of building block 3:

10-Phenyl-10*H*-phenothiazine, 1:[51] A solution of the corresponding phenothiazine (1.99 g, 10 mmol) and aryl bromide (1 mL, 11 mmol) in toluene (10 mL) was added to an oven-dried sealed tube equipped with a magnetic stir bar, followed by addition of $Pd_2(dba)_3$ (275 mg, 0.3 mmol), $[(^tBu)_3PH]BF_4$ (145 mg, 0.5 mmol) and NaO^tBu (1.11 g, 11.5 mmol). The reaction was refluxed for 48 h under inert atmosphere and monitored by TLC (phosphomolybdic acid stain solution). Then, the mixture was cooled to room temperature, diluted with DCM (20 mL), and filtered through a plug of celite. The filter cake was washed with DCM (2 x 10 mL), and the filtrate was concentrated under reduced pressure. The resulting crude mixture was purified by flash column chromatography (*c*-Hex) to provide **1** (78 % yield). ^{1}H-NMR (300 MHz, $CDCl_3$) δ 7.62 (t, J = 7.7 Hz, 2H), 7.52-7.50 (m, 1H), 7.42 (dd, J = 8.3, 1.1 Hz, 2H), 7.05 (dd, J = 6.7,

2.4 Hz, 2H), 6.87-6.83 (m, 4H), 6.23 (dd, J = 7.6, 1.6 Hz, 2H) ppm. ^{13}C-NMR (75 MHz, $CDCl_3$) δ 144.4, 141.1, 130.9, 130.8, 128.3, 126.9, 126.8, 122.6, 120.3, 116.2 ppm.

3,7-Dibromo-10-(4-bromophenyl)-10*H*-phenothiazine, 2: A solution of *N*-bromo-succinimide (3.11 g, 1.75 mmol) in THF (40 mL) was added dropwise to a round flask equipped with a magnetic stir bar and a solution of **1** (1.38 g, 0.5 mmol) in THF (10 mL). The reaction was stirred in an ice bath for 3 h and monitored by TLC. Then, NaOH 3 M (20 mL) was added to the reaction mixture, and it was extracted with 3x20 mL of AcOEt. The organic phase was separated, dried by $MgSO_4$, filtrated, and evaporated under reduced pressure. The resulting crude mixture was purified by flash column chromatography (*c*-Hex/AcOEt = 99:1 vol/vol) to provide **2** (60% yield). ^{1}H-NMR (300 MHz, $CDCl_3$) δ 7.74 (d, J = 8.7 Hz, 2H), 7.23 (d, J = 8.7 Hz, 2H) 7.12 (d, J = 2.3 Hz, 2H), 6.94 (dd, J = 8.8, 2.3 Hz, 2H), 6.02 (d, J = 8.8 Hz, 2H) ppm. ^{13}C-NMR (75 MHz, $CDCl_3$) δ 142.9, 139.5, 134.6, 132.3, 130.0, 129.2, 122.8, 122.0, 117.4, 115.3 ppm.

10-(4-Formylphenyl)-10*H*-phenothiazine-3,7-dicarbaldehyde, building block 3: A solution of **2** (450 mg, 0.90 mmol) in dry THF (12 mL) was stirred in a round flask with a magnetic stir bar under inert atmosphere. Keeping the inert atmosphere at -78°C, *n*-BuLi 1.6 M (2.2 mL) was added dropwise to the reaction mixture for 1 h. After that, still at -78°C, dry DMF (0.27 mL) was added, and the reaction was stirred for 3 h. Finally, HCl 1.2 M (6 mL) was added to quench the reaction mixture at 0°C, and it was stirred for 30 minutes. The reaction mixture was extracted with 5x20 mL of DCM. The organic phase was separated, dried by $MgSO_4$, filtrated, and evaporated under reduced pressure. The resulting crude mixture was purified by flash column chromatography (*c*-Hex/AcOEt = 99:1 vol/vol) to provide **3** (96% yield). Orange solid. ^{1}H-NMR (300 MHz, $CDCl_3$) δ 10.17 (s, 1H), 9.75 (s, 2H) 8.22 (d, J = 8.1 Hz, 2H), 7.60 (d, J = 7.9 Hz, 2H), 7.51 (s, 2H), 7.33 (dd, J = 8.5, 1.8 Hz, 2H), 6.17 (d, J = 8.5 Hz, 2H) ppm. ^{13}C-

NMR (75 MHz, $CDCl_3$) δ 190.6, 189.5, 146.8, 144.7, 136.8, 132.7, 132.4, 131.3, 129.9, 127.7, 120.6, 116.1 ppm.

Synthesis of COF 4a-e: A solvothermal reactor was charged with 1,3,5-tris(4-aminophenyl)benzene (**TAPB**) (50.0 mg, 0.14 mmol), and different proportions of the synthesized building block **3** or/and tris(4-formylphenyl)amine (**TFPA**), 0.6 mL of anhydrous dioxane, 5.4 mL of mesitylene and 0.6 mL of 6 M acetic acid in water. The reactor was heated at 120 ˚C for 72 h, yielding a solid which was isolated by filtration and washed with DMF, MeOH and THF. The resulting powder was immersed in anhydrous THF for 24 h and dried first at room temperature under vacuum for 12 h, and then at 100 ˚C for 2 h to afford an orange-yellow powder. For the characterization, see Supporting Information.

General procedure for the photodegradation of PBDE-1: An oven-dried 10 mL vial equipped with a magnetic stir bar was charged with photocatalyst COF **4a-e** (1 mg) and polybrominated diphenyl ether 1 (PBDE-1) (8.3 mg, 0.033 mmol). Then, acetonitrile (1 mL) and DIPEA (14.2 μL, 0.08 mmol) were added. The vial was closed with a rubber septum and the reaction mixture was degassed by three cycles vacuum / argon of "freeze-pump-thaw". The vial was placed on the blue light LED photoreactor (420 nm) and the reaction mixture was stirred at 25 ˚C. The reaction was checked by ^{1}H-NMR after 24 hours. The crude was filtered through membrane filter and purified by flash chromatography.

Leaching test: An oven-dried 10 mL vial equipped with a magnetic stir bar was charged with photocatalyst **4e** (1 mg) and PBDE-1 (8.3 mg, 0.033 mmol). Then, acetonitrile (1 mL) and DIPEA (14.2 μL, 0.08 mmol) were added. The vial was closed with a rubber septum and the reaction mixture was degassed by three cycles vacuum / argon of "freeze-pump-thaw". Then the vial was placed on the blue light LED photoreactor (420 nm) and the reaction mixture was stirred at 25 ˚C for 24 h. The conversion was determined by ^{1}H-NMR analysis of the crude mixture. Then, the vial was opened, and the crude mixture was filtered through membrane filter.

PBDE-1 (8.3 mg, 0.033 mmol) and DIPEA (14.2 μL, 0.08 mmol) were added again for a next run without photocatalyst COF. The previous conversion was determined by ^{1}H-NMR analysis of the crude mixture. The vial was closed, and the reaction mixture was degassed following the same procedure than before. After 24 h, the conversion of the crude mixture was determined by ^{1}H-NMR analysis, and it was shown that there was no photodegradation (see Supporting Information).

Recyclability test: An oven-dried 10 mL vial equipped with a magnetic stir bar was charged with photocatalyst **4e** (1 mg) and PBDE-1 (8.3 mg, 0.033 mmol). Then, acetonitrile (1 mL) and DIPEA (14.2 μL, 0.08 mmol) were added. The vial was closed with a rubber septum and the reaction mixture was degassed by three cycles vacuum / argon of "freeze-pump-thaw". Then the vial was placed on the blue light LED photoreactor (420 nm) and the reaction mixture was stirred at 25 ˚C for 24 h. The conversion was determined by ^{1}H-NMR analysis of the crude mixture. Then, the vial was opened and PBDE-1 (8.3 mg, 0.033 mmol) and DIPEA (14.2 μL, 0.08 mmol) were added again for a next run. After that, the vial was closed, and the reaction mixture was degassed following the same procedure than before. Seven consecutive cycles have been carried out.

General procedure for the photodegradation of Sudan Red III: A 30 mL screw vial equipped with a magnetic stir bar was charged with photocatalyst COF **4a-e** (2 mg) and the dye Sudan Red III (1.25 x 10^{-2} mM) in toluene (10 mL). Then, the mixture was sonicated to disperse the COF. The closed vial was placed under the blue spotlight and the reaction mixture was stirred at room temperature. The photodegradation was determined by UV-Vis spectrophotometer after 34 hours.

General procedure for the photodegradation of Methylene Blue: A 30 mL screw vial equipped with a magnetic stir bar was charged with photocatalyst COF **4a-e** (2 mg) and the dye Methylene Blue (2.25 x 10^{-2} mM) in acetonitrile (20 mL). Then, the mixture was sonicated to

disperse the COF. The closed vial was placed under the blue spotlight and the reaction mixture was stirred at room temperature. The photodegradation was determined by UV-Vis spectrophotometer after 4 hours.

Mechanistic experiments: A 30 mL screw vial equipped with a magnetic stir bar was charged with photocatalyst **4e** (2 mg) and the dye Sudan Red III (1.25 x 10^{-2} mM) in toluene (10 mL) or with photocatalyst COF **4a** (2 mg) and the dye Methylene Blue (2.25 x 10^{-2} mM) in acetonitrile (20 mL). DABCO or benzoquinone were added (5 equiv.) to the reaction mixture. Then, the mixture was sonicated to disperse the COF. Another vial was closed with a rubber septum and the reaction mixture was degassed by three cycles vacuum / argon of "freeze-pump-thaw". Then, all closed vials were placed under the blue spotlight. The reaction mixture was stirred at room temperature. The photodegradation was determined by UV-Vis spectrophotometer after 20 hours for Sudan Red III and after 3 hours in the case of Methylene Blue.

3. Results and Discussion

3.1. Synthesis and characterization.

The synthetic strategy followed in this work is presented in Scheme 2. We initially started with the synthesis of a new building block, 10-(4-formylphenyl)-10*H*-phenothiazine-3,7-dicarbaldehyde (**3**), containing the phenyl phenothiazine (PTH) unit. This unit is a known homogeneous photocatalyst with excellent redox properties (oxidation potential at the excited state: -2.1 V *vs* SCE),[52] and it is able to catalyze different photochemical processes, such as hydrodehalogenation,[52] halogenation,[53] oxidative coupling of primary amines [54] and photopolymerization processes.[55] The building block **3** was synthesized in three steps (Scheme 1), starting from phenothiazine and aryl bromide.

Then, the resulting intermediate was brominated with *N*-bromo-succinimide. Finally, **3** was generated by the reaction of brominated intermediate in the presence of *n*-butyllithium 1.6 M with dry DMF at -78 °C, followed by treatment with HCl 1.2 M at 0 °C. Thus, **3** was obtained as an orange solid after flash-column chromatography purification.

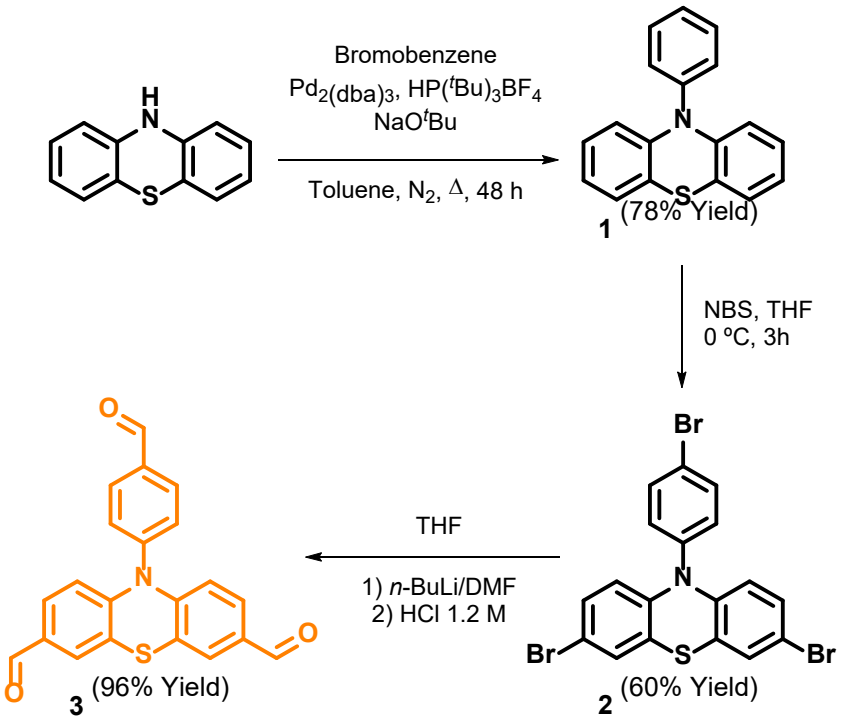

Scheme 1. Synthesis of the new building block **3** based on PTH.

We then synthesized the five COFs **4a-e** by solvothermal reaction of mixtures of variable relative amounts of **3** and tris(4-formylphenyl)amine (**TFPA**) with the trianiline precursor **TAPB** (Scheme 2). The feasibility of this design lays on the fact that both building blocks (**3** and **TFPA**) impose very similar geometric constraints, being possible to substitute one by the other without major distortion of the laminar COF structure. In this series, we synthesized COF **4a** using only **TFPA**,[56,57] and material **4e** using **3**, to compare the photocatalytic activity of TPA and PTH units embedded into the polyimine

frameworks. In addition, we isolated three more mixed-photoactive-linker COFs **4b-d** containing mixtures of **3** and **TFPA** (ratio TPA/PTH: 7, 3 and 1, see Table 1).

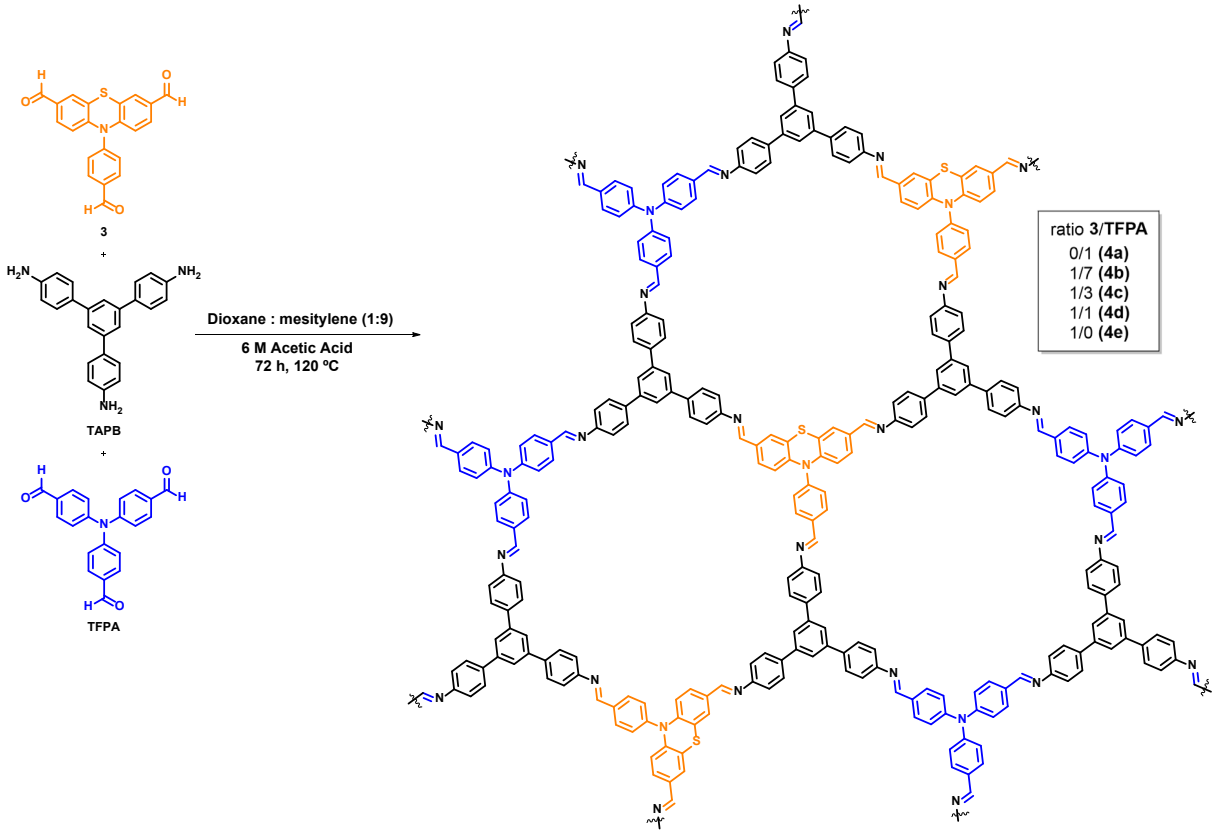

Scheme 2. Synthesis of the series of COFs **4a-e**, which were obtained by variating the **TFPA/3** molar ratio.

Table 1. Proportion of **3** and **TFPA** used in the synthesis of COFs **4a-e**.[a]

Material	mol % of **3**	mol % of **TFPA**	Ratio **3**/**TFPA**	Elemental Analysis[b] (S %)[c]
4a	0	100	0/1	0.03 (0.00)
4b	12.5	87.5	1/7	0.42 (0.59)
4c	25	75	1/3	1.21 (1.17)
4d	50	50	1/1	2.20 (2.31)
4e	100	0	1/0	4.67 (4.51)

[a] All materials were prepared in solvothermal reactors charged with **TAPB** (0.14 mmol), the corresponding proportion (0.14 mmol) of the synthesized **3** or/and **TFPA**, 2.7 mL of anhydrous

dioxane and 0.6 mL of 3 M acetic acid in water, at 120 ˚C for 72 h. [b] Experimental value. [c] Expected values are included in brackets.

The formation and quality of synthesized COFs **4a-e** were studied by powder X-ray diffraction (PXRD; Figure 2) and Brunauer-Emmett-Teller surface area (S_{BET}) measured by N_2 sorption analysis performed at 77 K (Figure 3). PXRD of COFs **4a-d** showed similar patterns indicating that comparable structures can be proposed for all of them. Using *Materials Studio 8.0* program, we compared these experimental PXRD data with the pattern simulated from the model structure of **4a** proposed by Jiang [56] and Verduzco.[57] Based on this structure, we applied a geometrical energy minimization using the universal force field. The unit cell parameters found for the eclipsed structure was a = 23.47 Å, b = 23.47 Å and c = 3.89 Å in a *P3* (nº 143) symmetry group. However, applying this model structure did not fit well with all our experimental PXRD peaks.[56] The major inconsistency consisted in an additional strong peak at 5.5 °. To this respect, Lukose *et al*. proposed in different COFs that inclined stacking of the layers can originate this peak.[58] Based on this hypothesis, we applied a geometrical energy minimization in a model that considered this inclined stacking. We found unit cell parameters for the inclined eclipsed structure of a = 40.84 Å, b = 23.96 Å and c = 4.63 Å in a *P1* (nº 1) symmetry group. Consistently, the experimental PXRD for **4b-d** corresponded to the pattern simulated from inclined COF model (see Supporting Information, Tables S6 and S7). However, we observed a slight gradual decrease of all peaks when the proportion of **3** was increased in the COF formation, indicating the introduction of disorder in these structures. In fact, this evolution was clearly seen for **4e**, in which an amorphous material was obtained.

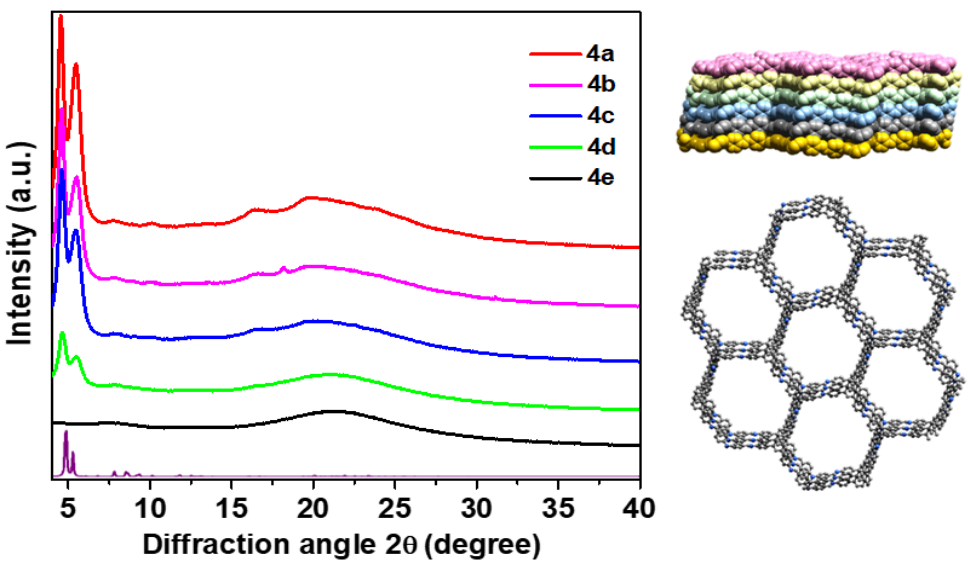

Figure 2. X-Ray diffractograms of **4a** (**red** data), **4b** (**pink**), **4c** (**blue**), **4d** (**green**) and **4e** (**black**) and the simulated X-Ray diffractogram of the model of **4a** considering an inclined stacking (**purple**).

These changes on the structural order were also consistent with the adsorption properties of the synthesized COFs (Figure 3). COF **4a** showed a S_{BET} of 522 $m^2 \cdot g^{-1}$ and a pore size distribution (calculated using a density functional theory (DFT) model (N_2 –cylindrical pores–oxide surface) with a main peak at 1.6 nm (see Supporting Information, Figure S35), which are in good agreement with the reported values.[56] However, when the proportion of **3** increased to 12.5 % in **4b**, 25 % in **4c**, 50 % in **4d** and 100 % in **4e**, the S_{BET} decreased to 386 $m^2 \cdot g^{-1}$, 382 $m^2 \cdot g^{-1}$, 126 $m^2 \cdot g^{-1}$ and 10 $m^2 \cdot g^{-1}$, respectively.

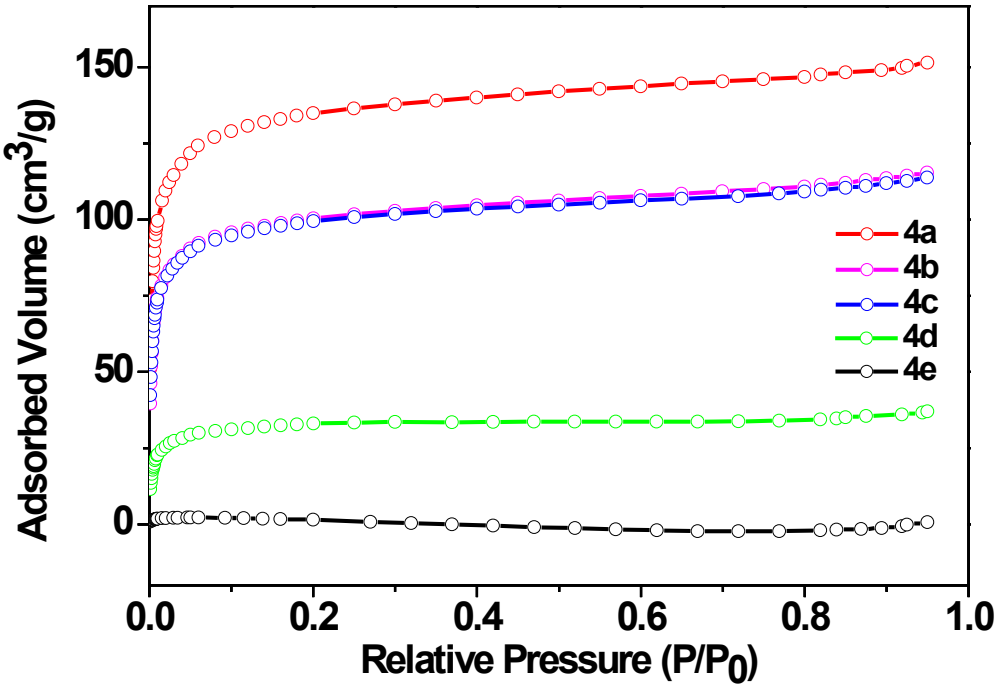

Figure 3. N_2 adsorption isotherm of **4a** (**red** data), **4b** (**pink**), **4c** (**blue**), **4d** (**green**) and **4e** (**black**).

The relative content of PTH in COFs **4a-e** was determined by elemental analysis (Table 1). The sulfur percentage detected was in good agreement with the expected values considering the proportions of **3** and **TFPA** used in each reaction. This result confirmed that there is not a preference for one or another building block, being both completely exchangeable. Analysis of the chemical structure was completed by IR and ^{13}C-CP-MAS-NMR (see Supporting Information, Figures S10 to S14 and S24 to S28). IR showed the typical vibration bands associated to imine groups, and NMR showed the expected signals in the aromatic region together with the iminic carbons. Therefore, altogether these characterization results were fully consistent with the formation of the pre-designed 2D hexagonally-ordered polyimine structures (Scheme 2). In addition, their microstructure was examined by Scanning Electron Microscopy (SEM), in which the hexagonal symmetry of the 2D structures was readily observed as hexagonal platelets

in all synthesized COFs (Figure 4). Finally, thermogravimetric analysis (TGA) revealed an excellent thermal stability of the 5 materials synthesized. In the case of COF **4a**, a slight decrease on its thermal stability (up to 430 ºC) was observed in comparison with materials containing PTH unit **4b-4e** (up to 495 ºC) (see Supporting Information, Figures S51 to S55).

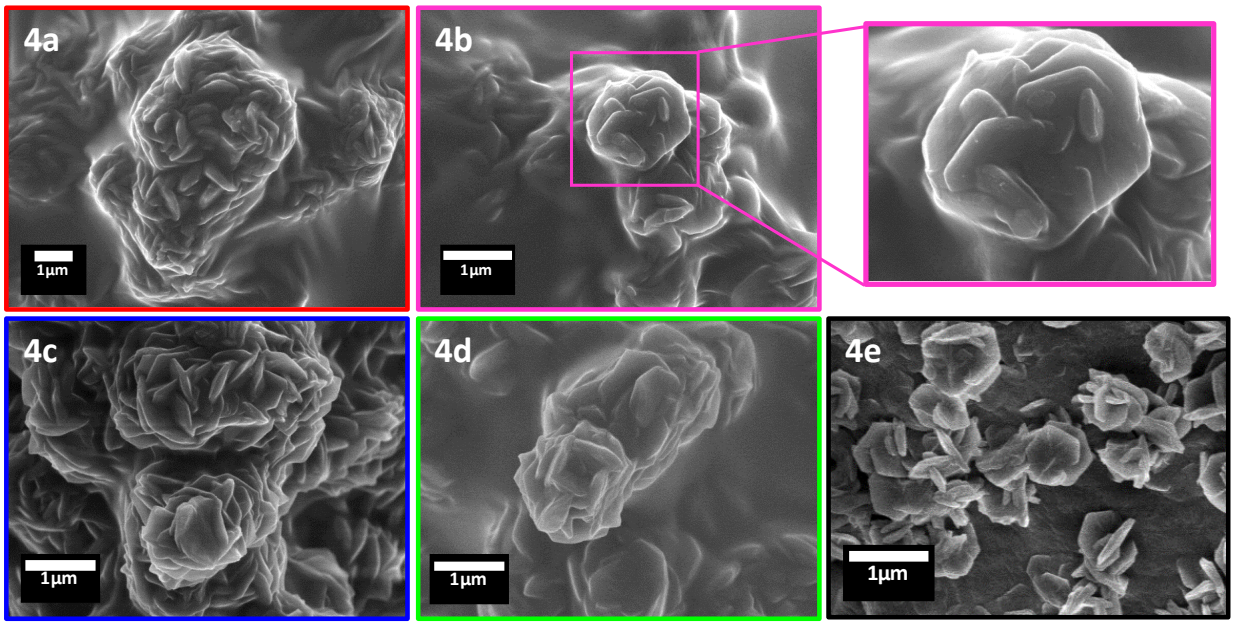

Figure 4. SEM images of COFs **4a** (**red**), **4b** (**pink**), **4c** (**blue**), **4d** (**green**) and **4e** (**black**).

Study of the optical properties of **4a-e** was carried out by means of diffuse reflectance and solid-state luminescence experiments. Figure 5a shows the absorption spectra normalized with the most intense peak in the region of 400-700 nm. Interestingly, the maximum absorption was dependent on the PTH/TPA content, being at 456 nm for the **TFPA**-based COF **4a** and at 504 nm for the material **4e** that only contains the tritopic aldehyde **3**.

Mixed-photoactive-linker COFs **4b-d** also showed mixed spectroscopic features. In normalized spectra, the absorption value of both signals appeared equally intense.

However, in non-normalized data (see inset in Figure 5a), it is clear that the absorption at 504 nm observed for **4e** is significantly more intense than the signal at 456 nm measured for **4a**. From these data, we have obtained the bandgap values of **4a-e** through Kubelka-Munk theory (2.33-2.25 eV, see supporting information for details).

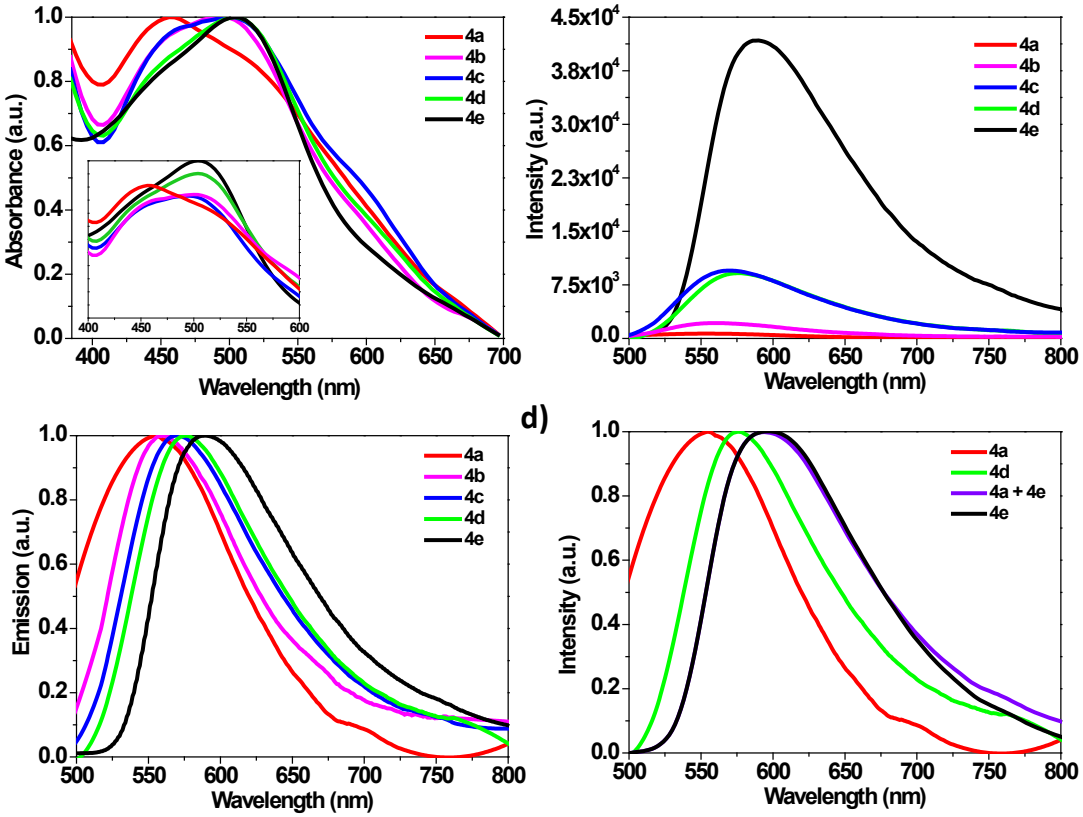

Figure 5. a) Absorption spectra of materials **4a** (**red**), **4b** (**pink**), **4c** (**blue**), **4d** (**green**) and **4e** (**black**). b) Non-normalized emission spectra. c) Normalized emission spectra. d) Comparison of normalized emission of materials **4a**, **4d** and **4e** with an equimolecular mixture of material **4a**+**4e**.

Emission experiments were fully consistent with the absorption data (Figure 5b-c). While the COF **4a** emitted with a maximum at 555 nm, the gradual enrichment of COFs **4b-d** with PTH induced a progressive redshift in the emission peak, which reached 590 nm for the PTH-based material **4e** (Figure 5c). Although an evident effect on the nature of the photoactive unit was found in the optical properties of the synthesized COFs, it is worth to mention that the data obtained are not uniquely due to PTH and TPA

units. In fact, molecular PTH and TPA building blocks (**3** and **TFPA**, respectively) absorb at significantly higher energies. Furthermore, emission is only observed for PTH containing building block **3** (at 530 nm), while **TFPA** does not emit at all (see Supporting Information, page S8). Therefore, the observed photophysical properties are the result of the electronic structure of the overall imine-based material, which is modulated by the distinct nature of TPA and PTH moieties. Taken together, optical data suggest that, by irradiating, TPA-based COF **4a** produces a more energetic excited state than PTH-containing COFs **4b-e**. These differences can be crucial to determine what type of photocatalytic process can be mediated by one or another COF.

In addition, we have compared the emission of materials **4a**, **4d** and **4e** with an equimolecular mixture of material **4a**+**4e**. As it can be seen in Figure 5d, the mixture of materials **4a**+**4e** shows an identical signal than pure **4e**. This is because the emission of **4a** is much less intense (see non-normalized emission, Figure 5b), and therefore, only the emission of **4e** was detected. These experiments and the emission of **4d** at lower wavelength demonstrated that this material (**4d**) is not composed from a mixture from **4a** and **4e** and it is just a hybrid material containing both building blocks **3** and **TFPA**.

Furthermore, we measured the energy of the Valence Band (VB) of **4a** and **4e** from the first oxidation signal of the cyclic voltammetry (see Supporting Information, Figures S43 and S44). Thus, we found that the VB energy level of **4a** is 4.90 eV and for **4e** is 4.54 eV. This indicates the easier tendency of material **4e** for triggering photoredox processes, which is in agreement with the observed catalytic activity (see below).

3.2. Determination of specific activity of each COF towards degradation of PBDE-1, Sudan Red III and Methylene Blue.

Prompted by the distinctive optical properties of COFs **4a-e**, we decided to compare their photocatalytic activity towards three processes of different nature. In particular, we studied the photodegradation of three pollutants: PBDE-1, Sudan Red III and Methylene Blue (Figure 1). The initial conditions used for the photocatalytic degradation of these pollutants were based on some precedents using other photoactive materials. [59–61] Moreover, we determined the optimal reaction times by an initial assessment of the kinetics of each reaction. For this purpose, we chose **4e** as the initial model photocatalytic material (see Supporting Information).

A first experiment was carried out adding 1 mg of **4e** in 1 mL of acetonitrile containing PBDE-1 (8.3 mg, 0.033 mmol) and *N*,*N*-diisopropylethylamine (DIPEA; 14.2 μL, 0.08 mmol), and irradiating the resulting mixture under blue light irradiation (450 nm LED) in an inert atmosphere for 24 h (see Supporting Information). To our delight, we observed that the use of **4e** resulted in the hydrodebrominated product in good yield (85%) after this reaction time. The degradation did not proceed in the absence of the photocatalytic material **4e** or without irradiation. In order to compare the photocatalytic activity of the remaining COFs (**4a-d**), they were also tested for 24 h under identical conditions. The results of these experiments are presented in Figure 6. As can be seen for the black trace in Figure 6, the best catalytic material for the hydrodebromination of PBDE-1 was **4e**, which only contains PTH as photoactive unit. We also found that COFs with lower proportion of PTH showed worst catalytic activities.

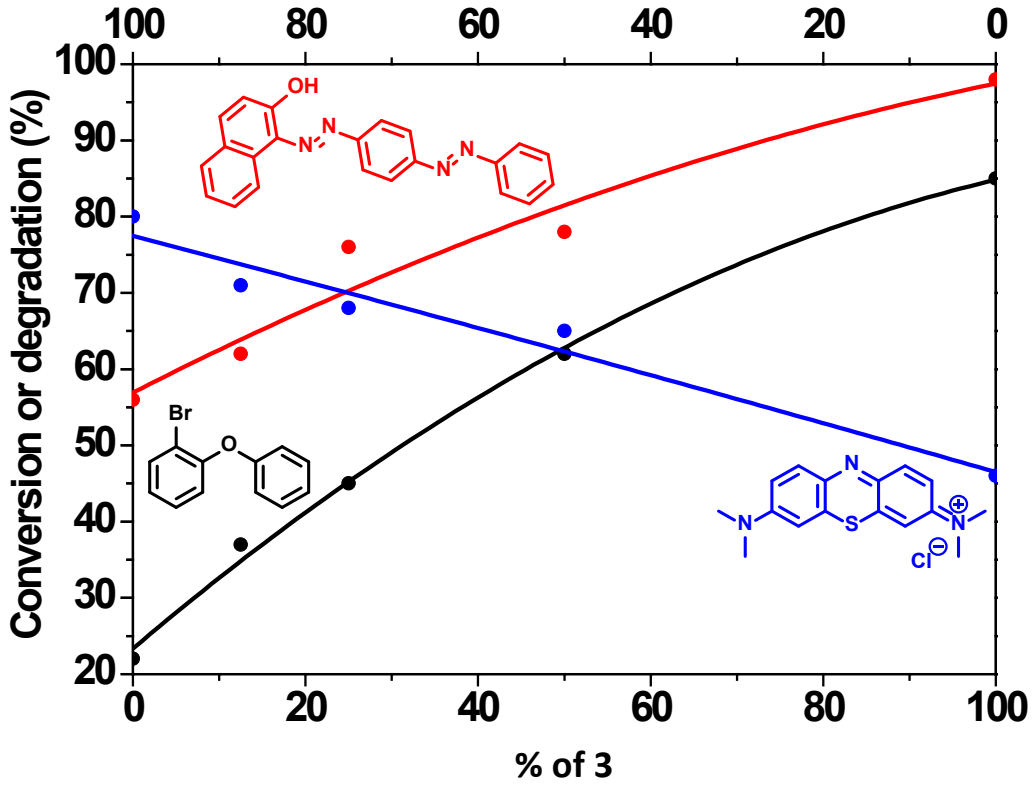

Figure 6. Conversion (%) of PBDE-1 to the debrominated product (black trace), and degradation (%) of Sudan Red III (red trace) and Methylene Blue (blue trace), using the five COFs **4a-e** (see Supporting Information for further details).

A similar set of experiments was carried out using 2 mg of **4e** under blue light irradiation for 34 h in 10 mL of toluene containing 1.25 x 10^{-2} mM of Sudan Red III. This substrate was almost completely degraded by **4e** after this reaction time. We also checked that the degradation barely progressed in the absence of the photocatalytic material **4e**, and it did not proceed at all in the absence of visible light. We also performed the comparative study of the different photoactivity depending on the proportion of **3** and **TFPA** employed in the synthesis of COFs **4a-d**. Under identical conditions, photodegradation of Sudan Red III using this series of COFs revealed that the catalytic

performance is also better when contain of PTH fragment is higher in the COF structure (red trace in Figure 6).

Finally, Methylene Blue photodegradation was studied using 2 mg of **4e** under blue light irradiation for 4 h in 20 mL of acetonitrile containing 2.25 x 10^{-2} mM of Methylene Blue (see Supporting Information). This pollutant was partially degraded by **4e** after this time (46 % degradation). In the absence of the photocatalytic material, the reaction also proceeded but with a much slower kinetics (12 % degradation after 4 h). In contrast, it did not progress at all in the absence of visible light (see Supporting Information). When we tested all COFs **4a-e** in the photodegradation of Methylene Blue under identical conditions, we observed the opposite trend than for PBDE-1 and Sudan Red III. In this case, the best result obtained was observed with COF **4a** that only contains TPA as the photoactive unit (80 % degradation after 4 h). These results suggest that, when the amount of TPA units increases in the structure of COFs, the degradation of Methylene Blue is more effective (blue trace in Figure 6). The high solubility of Methylene Blue in water allowed us to test the catalytic activity of **4a** and **4e**, founding a very similar behavior to the one observed in the organic solvent (see Supporting Information for kinetics).

Overall, a main observation of this work is that PTH and TPA units showed different preferences as photocatalyst in the studied systems. While activation of PBDE-1 and Sudan Red III are better performed by the PTH-containing material **4e**, photodegradation of Methylene Blue is better achieved by the TPA-based COF **4a**. Mixed-photoactive-linker COFs **4b-d** always showed intermediate catalytic results, indicating that no cooperative/synergistic effects are observed.

3.3. Mechanistic considerations

Photocatalytic hydrodebromination is a well-studied process [35,62] initiated by the electron transfer from the photocatalyst in its excited state to the organo-brominated substrate (Scheme 3a) and under inert atmosphere. Then, it readily evolves through the C-Br bond cleavage, producing the bromide anion and the corresponding organic radical species. Tertiary amines, such as DIPEA, act as the final reducing agent that ultimately closes the catalytic cycle, regenerating the starting photocatalytic material, and producing the corresponding amine radical cation. Finally, the radical organic intermediate evolves through a hydrogen atom transfer from the oxidized amine radical cation to finally generate the hydrodebrominated product and the iminium cation. In this process, the optimal performance of a photocatalyst is the result of the balance between the ability to perform two key steps: i) electron transfer from the photocatalyst in its excited state to the organo-brominated substrate; and ii) the reduction of oxidized photocatalyst by the sacrificial electron donor (DIPEA). While TPA-containing COF **4a** showed almost a negligible activity towards hydrodebromination of PBDE-1, PTH-based material **4e** was very active.

In the case of Sudan Red III degradation, the presence of oxygen was required. Thus, when this process was carried out under argon atmosphere, Sudan Red III did not react (Table 2, entries 1 and 2). Therefore, PTH-based material **4e** in its excited state must be able to activate O_2, resulting in the Sudan Red III oxidative degradation. Two different mechanisms are possible for this reaction: i) an energy transfer process, where singlet oxygen is the reactive species;[63] or ii) a photoredox process, where the transformation is mediated by superoxide radical anion.[64] Differentiation between these two mechanisms can be achieved by using additives that can act as selective scavengers, regardless the nature of the degraded substrate. In particular, quenching by

benzoquinone is indicative of a photoredox mechanism.[64,65] DABCO is another scavenger that can be used, which reacts with singlet oxygen, inhibiting the energy transfer pathway.[63,66]

Photodegradation of Sudan Red III was uniquely inhibited by addition of DABCO, indicating the involvement of singlet oxygen (Table 2, entries 3 and 4).

The degradation of Methylene Blue proceeds without the need of oxygen (Table 2, entries 5 and 6). Consistently, no specific quenching was found for this process when the reaction was carried out under open atmosphere in the presence of DABCO or benzoquinone (Table 2, entries 7 and 8). Considering that photodegradation of Methylene Blue works without any final oxidizing agent (such as oxygen) or reducing agent (such as DIPEA), the role of COFs should consist of transferring energy from its excited state to the Methylene Blue molecule. Such pathway implies that activated Methylene Blue molecule is able to spontaneously decompose after excitation. Consistently, Methylene Blue showed some level of degradation in the absence of photocatalytic material,[67] albeit slower than in the presence of photocatalytic COFs. In fact, Methylene Blue degradation reached 12 % value after 4 h under blue light irradiation in the absence of photocatalyst. Overall, the role of photocatalytic COFs is as photosensitizer acting as mediator in the excitation of Methylene Blue.

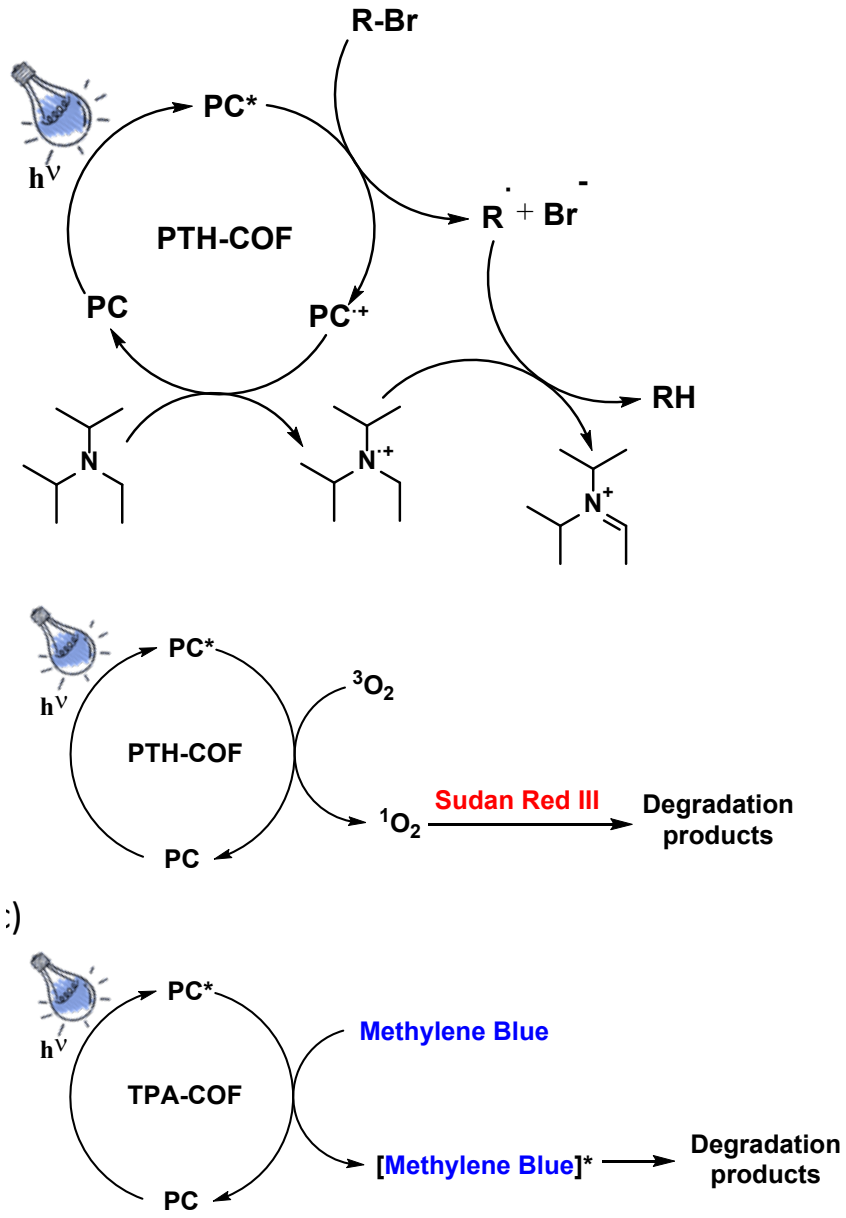

Scheme 3. Mechanistic proposals for the degradation of pollutants: a) PBDE-1, b) Sudan Red III, and c) Methylene Blue.

Table 2. Photodegradation of Sudan Red III[a] and Methylene Blue[b] under blue light irradiation with different reaction conditions.

Entry	Pollutant	Material	O_2/Ar	Additive[c]	(%) Degradation[d]
1	SR III	**4e**	O_2	-	48
2	SR III	**4e**	Ar	-	9
3	SR III	**4e**	O_2	DABCO	4
4	SR III	**4e**	O_2	BQ	45
5	MB	**4a**	O_2	-	60
6	MB	**4a**	Ar	-	59
7	MB	**4a**	O_2	DABCO	67
8	MB	**4a**	O_2	BQ	63

[a] All reactions were carried out using Sudan Red III (SR III) (1.25×10^{-2} mM) and 2 mg of **4e** as photocatalyst in 10 mL of toluene under blue light irradiation for 30 h. [b] All reactions were carried out using Methylene Blue (MB) (2.25×10^{-2} mM) and 2 mg of COF **4a** as photocatalyst in 20 mL of acetonitrile under blue light irradiation for 3 h. [c] 5 equivalents of DABCO and benzoquinone (BQ) additives were added. [d] Determined by UV-Vis spectrophotometer.

As conclusion, gradual replacement of PTH by TPA in the COFs resulted on a progressive inhibition of the photoredox process. According to spectroscopic data shown above (Figure 5), TPA-based COF **4a** absorbs and emits at higher energies than PTH-based material **4e**, indicating that more energetic excited states are generated. As a consequence, TPA units in this series of COFs enhances the efficiency on transferring energy to Methylene Blue, which has a singlet-triplet gap (1.36 eV) [68] higher than the $^3\Sigma_g$-$^1\Sigma_g$ energy difference for oxygen molecule (0.98 eV approx.),[69] which is effectively activated by **4e**.

4. Recyclability

The durability and recyclability of the photocatalytic materials were analyzed by considering as a model system the photodegradation of PDBE-1 catalyzed by **4e**. In order to discard leaching of active molecular fragments into the reaction medium, the crude mixture was filtered through membrane filter after a photocatalytic run of 24 h for the degradation of PBDE-1. Thereafter, PBDE-1 (0.033 mmol) and DIPEA (0.08 mmol) were added again to the filtered solution for a new run in the absence the photocatalytic material. In this case, NMR analysis showed that degradation did not progress after being irradiated in the absence of **4e** (see ESI).

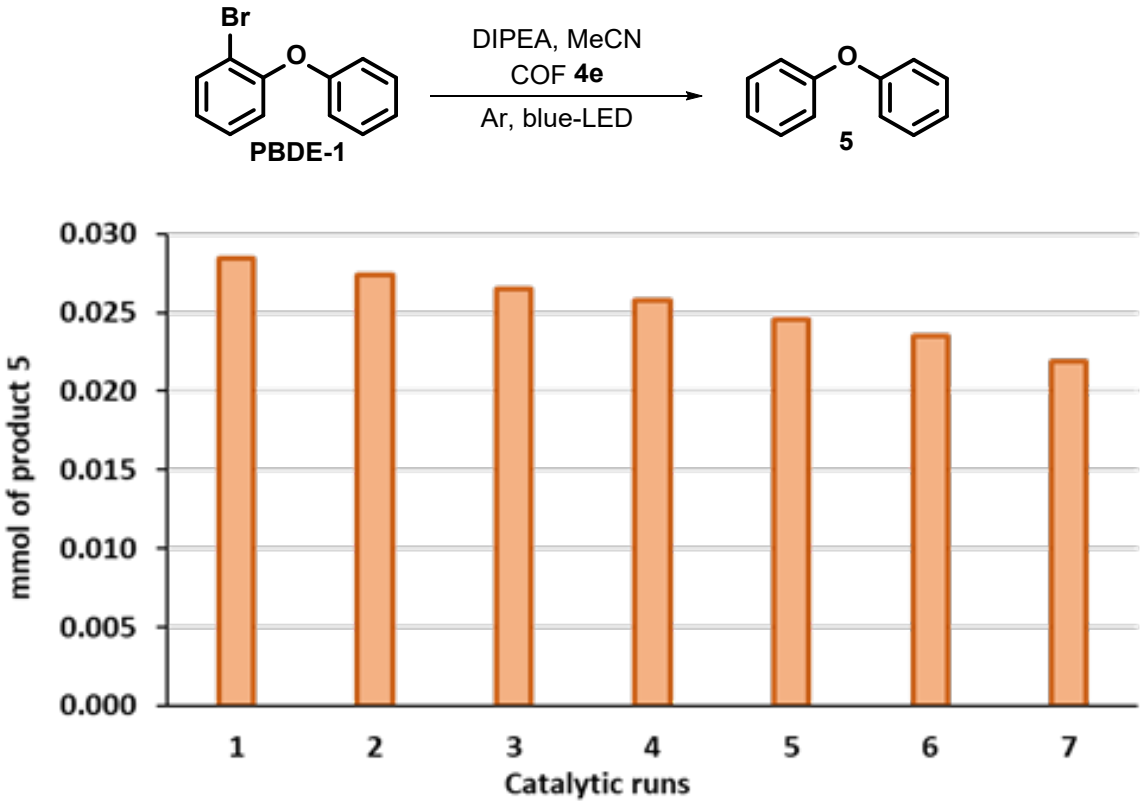

Figure 7. Photocatalytic runs in the photodegradation of PBDE-1 with **4e.**

With the aim of evaluating the recyclability of **4e**, we performed seven consecutive 24 h catalytic runs (total 168 h, Figure 7). Remarkably, only 1 mg of **4e** was able to degrade 0.178 mmol (44.3 mg) of PBDE-1. After one catalytic run, we analyzed the chemical integrity of **4e** by means of IR spectroscopy, observing that no degradation

was found after the catalytic reaction. In addition, SEM images confirmed that no structural erosion was found after one photocatalytic run. Moreover, the emission properties of **4e** were also totally conserved (see Supporting Information, Figures S4 and S5).

5. Conclusions

Two structurally analogous COFs with different properties were isolated by using two different building blocks **3** and **TFPA** containing PTH and TPA photoactive units, respectively. In addition, combination of both building blocks results on three additional mixed-photoactive-linker COFs with similar structures and intermediate physical and chemical characteristics. This synthetic strategy opens new avenues for developing a diverse variety of photoactive COFs showing good performances in different photodegradation processes, depending on the content of one or another photoactive unit. The COFs synthesized work under visible-light conditions without leaching of molecular fragments into the reaction media and show a high degree of recyclability and stability under the reaction conditions. In particular, they were able to efficiently perform the photodegradation of three pollutants of distinct nature: PBDE-1, Sudan Red III and Methylene Blue. PTH-based material **4e** was the best catalyst for the photoredox degradation of PBDE-1. However, efficiency of processes triggered by energy transfer to different chemical species are highly dependent on the PTH/TPA relative content. Thus, energy transfer to Methylene Blue was better achieved by TPA-based COF **4a**, whereas singlet oxygen generation works better using PTH-based material **4e**, resulting in the degradation of Sudan Red III. Overall, this work expands the use of COFs in a wide range of photocatalytic transformations and contributes to the design of innovative strategies to modulate and direct the activity of photocatalytic porous materials.

Competing financial interests

The authors declare no competing financial interests.

Acknowledgements

Financial support was provided by the European Research Council (ERC-CoG, contract number: 647550), Spanish Government (PID2019-110637RB-I00, RTI2018-095038-B-I00 and RTI2018-095622-B-I00), "Comunidad de Madrid" and European Structural Funds (S2018/NMT-4367). It was also funded by the CERCA Program/Generalitat de Catalunya. ICN2 is supported by the Severo Ochoa program from the Spanish MINECO (Grant No. SEV-2017-0706). Alberto López-Magano thanks to UAM for FPI-UAM predoctoral fellowship.

Apendix A

Electronic Supplementary Information

References

[1] P. Venkata Laxma Reddy, K.H. Kim, Y.H. Kim, A review of photocatalytic treatment for various air pollutants, Asian J. Atmos. Environ. 5 (2011) 181–188. https://doi.org/10.5572/ajae.2011.5.3.181.

[2] N.J. Turro, Energy Transfer Processes, Pure Appl. Chem. 49 (1977) 405–429.

[3] C.R.J. Stephenson, Y. Tehshik P, D.W.C. MacMillan, Visible Light Photocatalysis in Organic Chemistry, Wiley - VCN Verlag GmbH Co. KGaA. (2018).

[4] J. Twilton, C. (Chip) Le, P. Zhang, M.H. Shaw, R.W. Evans, D.W.C. MacMillan, The

merger of transition metal and photocatalysis, Nat. Rev. Chem. 1 (2017) 52. https://doi.org/10.1038/s41570-017-0052.

[5] N.A. Romero, D.A. Nicewicz, Organic Photoredox Catalysis, Chem. Rev. 116 (2016) 10075–10166. https://doi.org/10.1021/acs.chemrev.6b00057.

[6] S.G.E. Amos, M. Garreau, L. Buzzetti, J. Waser, Photocatalysis with organic dyes: Facile access to reactive intermediates for synthesis, Beilstein J. Org. Chem. 16 (2020) 1163–1187. https://doi.org/10.3762/bjoc.16.103.

[7] R. Ameta, S. Benjamin, A. Ameta, S.C. Ameta, Photocatalytic degradation of organic pollutants: A review, Mater. Sci. Forum. 734 (2013) 247–272. https://doi.org/10.4028/www.scientific.net/MSF.734.247.

[8] N. Hoffmann, Photochemical Reactions as Key Steps in Organic Synthesis, Chem. Rev. 108 (2008) 1052–1103. https://doi.org/10.1021/cr0680336.

[9] S. Gisbertz, B. Pieber, Heterogeneous Photocatalysis in Organic Synthesis, ChemPhotoChem. 4 (2020) 456–475. https://doi.org/https://doi.org/10.1002/cptc.202000014.

[10] J.-D. Xiao, H.-L. Jiang, Metal–Organic Frameworks for Photocatalysis and Photothermal Catalysis, Acc. Chem. Res. 52 (2019) 356–366. https://doi.org/10.1021/acs.accounts.8b00521.

[11] G.-B. Wang, S. Li, C.-X. Yan, F.-C. Zhu, Q.-Q. Lin, K.-H. Xie, Y. Geng, Y.-B. Dong, Covalent organic frameworks: emerging high-performance platforms for efficient photocatalytic applications, J. Mater. Chem. A. 8 (2020) 6957–6983. https://doi.org/10.1039/D0TA00556H.

[12] J. Wang, S. Zhuang, Covalent organic frameworks (COFs) for environmental applications, Coord. Chem. Rev. 400 (2019) 213046. https://doi.org/https://doi.org/10.1016/j.ccr.2019.213046.

[13] A. López-Magano, A. Jiménez-Almarza, J. Alemán, R. Mas-Ballesté, Metal–Organic Frameworks (MOFs) and Covalent Organic Frameworks (COFs) Applied to Photocatalytic Organic Transformations, Catal. 10 (2020) 720 https://doi.org/10.3390/catal10070720.

[14] A.P. Côté, A.I. Benin, N.W. Ockwig, M. O'Keeffe, A.J. Matzger, O.M. Yaghi, Porous, Crystalline, Covalent Organic Frameworks, Science (80-.). 310 (2005) 1166 LP – 1170. https://doi.org/10.1126/science.1120411.

[15] R.K. Sharma, P. Yadav, M. Yadav, R. Gupta, P. Rana, A. Srivastava, R. Zbořil, R.S. Varma, M. Antonietti, M.B. Gawande, Recent development of covalent organic frameworks (COFs): synthesis and catalytic (organic-electro-photo) applications, Mater. Horizons. 7 (2020) 411–454. https://doi.org/10.1039/C9MH00856J.

[16] L. Zhu, Y.-B. Zhang, Crystallization of Covalent Organic Frameworks for Gas Storage Applications, Mol. . 22 (2017). https://doi.org/10.3390/molecules22071149.

[17] A.K. Mandal, J. Mahmood, J.-B. Baek, Two-Dimensional Covalent Organic Frameworks for Optoelectronics and Energy Storage, ChemNanoMat. 3 (2017) 373–391. https://doi.org/https://doi.org/10.1002/cnma.201700048.

[18] Q. Fang, J. Wang, S. Gu, R.B. Kaspar, Z. Zhuang, J. Zheng, H. Guo, S. Qiu, Y. Yan, 3D Porous Crystalline Polyimide Covalent Organic Frameworks for Drug Delivery, J. Am. Chem. Soc. 137 (2015) 8352–8355. https://doi.org/10.1021/jacs.5b04147.

[19] H. Ma, B. Liu, B. Li, L. Zhang, Y.-G. Li, H.-Q. Tan, H.-Y. Zang, G. Zhu, Cationic Covalent Organic Frameworks: A Simple Platform of Anionic Exchange for Porosity Tuning and Proton Conduction, J. Am. Chem. Soc. 138 (2016) 5897–5903. https://doi.org/10.1021/jacs.5b13490.

[20] S.-Y. Ding, J. Gao, Q. Wang, Y. Zhang, W.-G. Song, C.-Y. Su, W. Wang, Construction of Covalent Organic Framework for Catalysis: Pd/COF-LZU1 in Suzuki–Miyaura

Coupling Reaction, J. Am. Chem. Soc. 133 (2011) 19816–19822. https://doi.org/10.1021/ja206846p.

[21] J. Luis-Barrerra, R. Cano, G. Imani-Shakibaei, J. Heras-Domingo, J. Pérez-Carvajal, I. Imaz, D. Maspoch, X. Solans-Monfort, J. Alemán, R. Mas-Ballesté, Switching acidic and basic catalysis through supramolecular functionalization in a porous 3D covalent imine-based material, Catal. Sci. Technol. 9 (2019) 6007–6014. https://doi.org/10.1039/C9CY01527B.

[22] X. Wang, L. Chen, S.Y. Chong, M.A. Little, Y. Wu, W.-H. Zhu, R. Clowes, Y. Yan, M.A. Zwijnenburg, R.S. Sprick, A.I. Cooper, Sulfone-containing covalent organic frameworks for photocatalytic hydrogen evolution from water, Nat. Chem. 10 (2018) 1180–1189. https://doi.org/10.1038/s41557-018-0141-5.

[23] J. Chen, X. Tao, C. Li, Y. Ma, L. Tao, D. Zheng, J. Zhu, H. Li, R. Li, Q. Yang, Synthesis of bipyridine-based covalent organic frameworks for visible-light-driven photocatalytic water oxidation, Appl. Catal. B Environ. 262 (2020) 118271. https://doi.org/https://doi.org/10.1016/j.apcatb.2019.118271.

[24] L. Guo, S. Jin, Stable Covalent Organic Frameworks for Photochemical Applications, ChemPhotoChem. 3 (2019) 973–983. https://doi.org/10.1002/cptc.201900089.

[25] X. Kang, X. Wu, X. Han, C. Yuan, Y. Liu, Y. Cui, Rational synthesis of interpenetrated 3D covalent organic frameworks for asymmetric photocatalysis, Chem. Sci. 11 (2020) 1494–1502. https://doi.org/10.1039/C9SC04882K.

[26] J. Yuan, Q. Xia, W. Zhu, C. Wu, B. Wang, B. Liu, X. Yang, Y. Xu, H. Xu, Sunlight-Driven Synthesis of 1,2,4-Thiadiazoles via Oxidative Construction of a Nitrogen-Sulfur Bond Catalyzed by a Reusable Covalent Organic Framework, ChemPhotoChem. n/a (2020). https://doi.org/10.1002/cptc.201900263.

[27] S. Wang, Q. Sun, W. Chen, Y. Tang, B. Aguila, Y. Pan, A. Zheng, Z. Yang, L. Wojtas,

S. Ma, F.-S. Xiao, Programming Covalent Organic Frameworks for Photocatalysis: Investigation of Chemical and Structural Variations, Matter. 2 (2020) 416–427. https://doi.org/https://doi.org/10.1016/j.matt.2019.10.026.

[28] H. Xue, S. Xiong, K. Mi, Y. Wang, Visible-light degradation of azo dyes by imine-linked covalent organic frameworks, Green Energy Environ. (2021). https://doi.org/https://doi.org/10.1016/j.gee.2020.09.010.

[29] A. Jiménez-Almarza, A. López-Magano, L. Marzo, S. Cabrera, R. Mas-Ballesté, J. Alemán, Imine-Based Covalent Organic Frameworks as Photocatalysts for Metal Free Oxidation Processes under Visible Light Conditions, ChemCatChem. 11 (2019) 4916. https://doi.org/10.1002/cctc.201901061.

[30] S. Ren, R. Dawson, D.J. Adams, A.I. Cooper, Low band-gap benzothiadiazole conjugated microporous polymers, Polym. Chem. 4 (2013) 5585–5590. https://doi.org/10.1039/C3PY00690E.

[31] N. Kang, J.H. Park, K.C. Ko, J. Chun, E. Kim, H.W. Shin, S.M. Lee, H.J. Kim, T.K. Ahn, J.Y. Lee, S.U. Son, Tandem synthesis of photoactive benzodifuran moieties in the formation of microporous organic networks, Angew. Chemie - Int. Ed. 52 (2013) 6228–6232. https://doi.org/10.1002/anie.201300655.

[32] J.-X. Jiang, Y. Li, X. Wu, J. Xiao, D.J. Adams, A.I. Cooper, Conjugated Microporous Polymers with Rose Bengal Dye for Highly Efficient Heterogeneous Organo-Photocatalysis, Macromolecules. 46 (2013) 8779–8783. https://doi.org/10.1021/ma402104h.

[33] Z.J. Wang, S. Ghasimi, K. Landfester, K.A.I. Zhang, A conjugated porous poly-benzobisthiadiazole network for a visible light-driven photoredox reaction, J. Mater. Chem. A. 2 (2014) 18720–18724. https://doi.org/10.1039/C4TA03887H.

[34] S. Dadashi-Silab, H. Bildirir, R. Dawson, A. Thomas, Y. Yagci, Microporous

Thioxanthone Polymers as Heterogeneous Photoinitiators for Visible Light Induced Free Radical and Cationic Polymerizations, Macromolecules. 47 (2014) 4607–4614. https://doi.org/10.1021/ma501001m.

[35] A. López-Magano, A.E. Platero-Prats, S. Cabrera, R. Mas-Ballesté, J. Alemán, Incorporation of Photocatalytic Pt(II) Complexes into Imine-Based Layered Covalent Organic Frameworks (COFs) through Monomer Truncation Strategy, Appl. Catal. B Environ. 272 (2020) 119027. https://doi.org/https://doi.org/10.1016/j.apcatb.2020.119027.

[36] Z.J. Wang, S. Ghasimi, K. Landfester, K.A.I. Zhang, Molecular Structural Design of Conjugated Microporous Poly(Benzooxadiazole) Networks for Enhanced Photocatalytic Activity with Visible Light, Adv. Mater. 27 (2015) 6265–6270. https://doi.org/10.1002/adma.201502735.

[37] M. Liras, M. Iglesias, F. Sánchez, Conjugated Microporous Polymers Incorporating BODIPY Moieties as Light-Emitting Materials and Recyclable Visible-Light Photocatalysts, Macromolecules. 49 (2016) 1666–1673. https://doi.org/10.1021/acs.macromol.5b02511.

[38] S. Ghasimi, S.A. Bretschneider, W. Huang, K. Landfester, K.A.I. Zhang, A Conjugated Microporous Polymer for Palladium-Free, Visible Light-Promoted Photocatalytic Stille-Type Coupling Reactions, Adv. Sci. (Weinheim, Baden-Wurttemberg, Ger. 4 (2017) 1700101. https://doi.org/10.1002/advs.201700101.

[39] All POPs listed in the Stockholm Convention, (n.d.). http://www.pops.int/TheConvention/ThePOPs/AllPOPs/tabid/2509/Default.aspx (accessed October 6, 2020).

[40] U. Gill, I. Chu, J.J. Ryan, M. Feeley, Polybrominated diphenyl ethers: human tissue levels and toxicology., Rev. Environ. Contam. Toxicol. 183 (2004) 55–97.

https://doi.org/10.1007/978-1-4419-9100-3_3.

[41] A.O. Souza, M.J. Tasso, A.M.C. Oliveira, L.C. Pereira, F. V Duarte, D.P. Oliveira, C.M. Palmeira, D.J. Dorta, Evaluation of Polybrominated Diphenyl Ether Toxicity on HepG2 Cells – Hexabrominated Congener (BDE-154) Is Less Toxic than Tetrabrominated Congener (BDE-47), Basic Clin. Pharmacol. Toxicol. 119 (2016) 485–497. https://doi.org/https://doi.org/10.1111/bcpt.12598.

[42] J.D. Raff, R.A. Hites, Gas-phase reactions of brominated diphenyl ethers with OH radicals., J. Phys. Chem. A. 110 (2006) 10783–10792. https://doi.org/10.1021/jp0630222.

[43] B. Padhi, Pollution due to synthetic dyes toxicity & carcinogenicity studies and remediation, Int. J. Environ. Sci. 3 (2012) 940–955. https://doi.org/10.6088/ijes.2012030133002.

[44] B. de C. Ventura-Camargo, M.A. Marin-Morales, Azo Dyes: Characterization and Toxicity– A Review, Text. Light Ind. Sci. Technol. 2 (2015) 85–103.

[45] M. Hou, F. Li, X. Liu, X. Wang, H. Wan, The effect of substituent groups on the reductive degradation of azo dyes by zerovalent iron, J. Hazard. Mater. 145 (2007) 305–314. https://doi.org/https://doi.org/10.1016/j.jhazmat.2006.11.019.

[46] H. Pan, J. Feng, G.-X. He, C.E. Cerniglia, H. Chen, Evaluation of impact of exposure of Sudan azo dyes and their metabolites on human intestinal bacteria, Anaerobe. 18 (2012) 445–453. https://doi.org/https://doi.org/10.1016/j.anaerobe.2012.05.002.

[47] J. Ma, D. Huang, J. Zou, L. Li, Y. Kong, S. Komarneni, Adsorption of methylene blue and Orange II pollutants on activated carbon prepared from banana peel, J. Porous Mater. 22 (2015) 301–311. https://doi.org/10.1007/s10934-014-9896-2.

[48] T.M. Albayati, A.A. Sabri, R.A. Alazawi, Separation of Methylene Blue as Pollutant of Water by SBA-15 in a Fixed-Bed Column, Arab. J. Sci. Eng. 41 (2016) 2409–2415.

https://doi.org/10.1007/s13369-015-1867-7.

[49] L. Lan, F. Liu, Y. Dan, L. Jiang, Facile fabrication of triphenylamine-based conjugated porous polymers and their application in organic degradation under visible light, New J. Chem. 44 (2020) 2986–2995. https://doi.org/10.1039/C9NJ05500B.

[50] X. Kong, A.P. Kulkarni, S.A. Jenekhe, Phenothiazine-Based Conjugated Polymers: Synthesis, Electrochemistry, and Light-Emitting Properties, Macromolecules. 36 (2003) 8992–8999. https://doi.org/10.1021/ma035087y.

[51] A.F. Garrido-Castro, N. Salaverri, M.C. Maestro, J. Alemán, Intramolecular Homolytic Substitution Enabled by Photoredox Catalysis: Sulfur, Phosphorus, and Silicon Heterocycle Synthesis from Aryl Halides, Org. Lett. 21 (2019) 5295–5300. https://doi.org/10.1021/acs.orglett.9b01911.

[52] E.H. Discekici, N.J. Treat, S.O. Poelma, K.M. Mattson, Z.M. Hudson, Y. Luo, C.J. Hawker, J.R. de Alaniz, A highly reducing metal-free photoredox catalyst: design and application in radical dehalogenations, Chem. Commun. 51 (2015) 11705–11708. https://doi.org/10.1039/C5CC04677G.

[53] B. Ma, F. Lu, H. Yang, X. Gu, Z. Li, R. Li, H. Pei, D. Luo, H. Zhang, A. Lei, Visible Light Mediated External Oxidant Free Selective C5 Bromination of 8-Aminoquinoline Amides under Ambient Conditions, Asian J. Org. Chem. 8 (2019) 1136–1140. https://doi.org/https://doi.org/10.1002/ajoc.201900293.

[54] J.H. Park, K.C. Ko, E. Kim, N. Park, J.H. Ko, D.H. Ryu, T.K. Ahn, J.Y. Lee, S.U. Son, Photocatalysis by Phenothiazine Dyes: Visible-Light-Driven Oxidative Coupling of Primary Amines at Ambient Temperature, Org. Lett. 14 (2012) 5502–5505. https://doi.org/10.1021/ol302584y.

[55] S. Dadashi-Silab, X. Pan, K. Matyjaszewski, Phenyl Benzo[b]phenothiazine as a Visible Light Photoredox Catalyst for Metal-Free Atom Transfer Radical Polymerization, Chem.

– A Eur. J. 23 (2017) 5972–5977. https://doi.org/https://doi.org/10.1002/chem.201605574.

[56] L. Zhai, N. Huang, H. Xu, Q. Chen, D. Jiang, A backbone design principle for covalent organic frameworks: the impact of weakly interacting units on CO2 adsorption, Chem. Commun. 53 (2017) 4242–4245. https://doi.org/10.1039/C7CC01921A.

[57] D. Zhu, L.B. Alemany, W. Guo, R. Verduzco, Enhancement of crystallinity of imine-linked covalent organic frameworks via aldehyde modulators, Polym. Chem. 11 (2020) 4464–4468. https://doi.org/10.1039/D0PY00776E.

[58] B. Lukose, A. Kuc, T. Heine, The Structure of Layered Covalent-Organic Frameworks, Chem. – A Eur. J. 17 (2011) 2388–2392. https://doi.org/https://doi.org/10.1002/chem.201001290.

[59] X. Feng, H. Ju, T. Song, T. Fang, W. Liu, W. Huang, Highly Efficient Photocatalytic Degradation Performance of CsPb(Br1–xClx)3-Au Nanoheterostructures, ACS Sustain. Chem. Eng. 7 (2019) 5152–5156. https://doi.org/10.1021/acssuschemeng.8b06023.

[60] T. Aarthi, P. Narahari, G. Madras, Photocatalytic degradation of Azure and Sudan dyes using nano TiO2, J. Hazard. Mater. 149 (2007) 725–734. https://doi.org/https://doi.org/10.1016/j.jhazmat.2007.04.038.

[61] K.K. Senapati, C. Borgohain, K.C. Sarma, P. Phukan, Photocatalytic degradation of methylene blue in water using CoFe2O4–Cr2O3–SiO2 fluorescent magnetic nanocomposite, J. Mol. Catal. A Chem. 346 (2011) 111–116. https://doi.org/https://doi.org/10.1016/j.molcata.2011.07.001.

[62] D. González-Muñoz, A. Casado-Sánchez, I. del Hierro, S. Gómez-Ruiz, S. Cabrera, J. Alemán, Size-selective mesoporous silica-based Pt(II) complex as efficient and reusable photocatalytic material, J. Catal. 373 (2019) 374–383. https://doi.org/https://doi.org/10.1016/j.jcat.2019.04.015.

[63] P.R. Ogilby, Singlet oxygen: there is indeed something new under the sun, Chem. Soc. Rev. 39 (2010) 3181–3209. https://doi.org/10.1039/B926014P.

[64] M. Hayyan, M.A. Hashim, I.M. AlNashef, Superoxide Ion: Generation and Chemical Implications, Chem. Rev. 116 (2016) 3029–3085. https://doi.org/10.1021/acs.chemrev.5b00407.

[65] R.I. Samoilova, A.R. Crofts, S.A. Dikanov, Reaction of Superoxide Radical with Quinone Molecules, J. Phys. Chem. A. 115 (2011) 11589–11593. https://doi.org/10.1021/jp204891n.

[66] C. Ouannes, T. Wilson, Quenching of singlet oxygen by tertiary aliphatic amines. Effect of DABCO (1,4-diazabicyclo[2.2.2]octane), J. Am. Chem. Soc. 90 (1968) 6527–6528. https://doi.org/10.1021/ja01025a059.

[67] Y. Xu, X. Shi, R. Hua, R. Zhang, Y. Yao, B. Zhao, T. Liu, J. Zheng, G. Lu, Remarkably catalytic activity in reduction of 4-nitrophenol and methylene blue by Fe3O4@COF supported noble metal nanoparticles, Appl. Catal. B Environ. 260 (2020) 118142. https://doi.org/https://doi.org/10.1016/j.apcatb.2019.118142.

[68] V.Y. Gak, V.A. Nadtochenko, J. Kiwi, Triplet-excited dye molecules (eosine and methylene blue) quenching by H2O2 in aqueous solutions, J. Photochem. Photobiol. A Chem. 116 (1998) 57–62. https://doi.org/https://doi.org/10.1016/S1010-6030(98)00230-5.

[69] G.P. Brasseur, S. Solomon, Aeronomy of the Middle Atmosphere, Springer, Springer Science & Business Media, 2005. https://www.springer.com/gp/book/9781402032844.